Journal of Structural Biology 168 (2009) 419–425

Contents lists available at ScienceDirect

Journal of Structural Biology

journal homepage: www.elsevier.com/locate/yjsbi

Cryo-electron tomography of nanoparticle transmigration into liposome

Olivier Le Bihan [a], Pierre Bonnafous [a], Laszlo Marak [b], Thomas Bickel [c], Sylvain Trépout [a,1], Stéphane Mornet [d], Felix De Haas [e], Hugues Talbot [b], Jean-Christophe Taveau [a], Olivier Lambert [a,*]

[a] Structure of Membrane Complexes and Cell Process, CBMN UMR-CNRS 5248, Université Bordeaux, ENITAB, IECB, Avenue des Facultés, F-33405 Talence, France
[b] ESIEE, BP99, 2 Bd Blaise Pascal, F-93162 Noisy-le-Grand Cedex, France
[c] CPMOH, Université Bordeaux, 316 cours de la Libération, F-33405 Talence, France
[d] ICMCB, CNRS, Université Bordeaux, 87 Avenue du Dr. A. Schweitzer, F-33608 Pessac, France
[e] FEI Electron Optics B.V. Achtseweg Noord 5, 5651 GG Eindhoven, The Netherlands

ARTICLE INFO

Article history:
Received 10 April 2009
Accepted 2 July 2009
Available online 23 July 2009

Keywords:
Liposome
Cryo-electron microscopy
Cryo-electron tomography
Nanoparticle
Nanoparticle transport

ABSTRACT

Nanoparticle transport across cell membrane plays a crucial role in the development of drug delivery systems as well as in the toxicity response induced by nanoparticles. As hydrophilic nanoparticles interact with lipid membranes and are able to induce membrane perturbations, hypothetic mechanisms based on membrane curvature or hole formation have been proposed for activating their transmigration. We report on the transport of hydrophilic silica nanoparticles into large unilamellar neutral DOPC liposomes via an internalization process. The strong adhesive interactions of lipid membrane onto the silica nanoparticle triggered liposome deformation until the formation of a curved neck. Then the rupture of this membrane neck led to the complete engulfment of the nanoparticle. Using cryo-electron tomography we determined 3D architectures of intermediate steps of this process unveiling internalized silica nanoparticles surrounded by a supported lipid bilayer. This engulfing process was achieved for a large range of particle size (from 30 to 200 nm in diameter). These original data provide interesting highlights for nanoparticle transmigration and could be applied to biotechnology development.

1. Introduction

The growing interest for nanoparticles is motivated by potential developments in nanotechnology, biotechnology or in medicine, but is also due to the health risk associated with their use (Nel et al., 2006). Indeed, toxicological effects have been already identified and further investigations are required to examine fundamental mechanisms underlying these undesirable biological responses. Among predictive pathways leading to nanoparticle toxicity, transmigration of nanoparticles into cell is one of main concerns.

Transport of nanoparticles into mammalian cells was proposed to be mediated by a non endocytotic pathway as evidenced by the entry of ultrafine particles within red blood cell and cyt-D – blocked macrophages that both lack of endocytotic capabilities (Geiser et al., 2005; Rothen-Rutishauser et al., 2006). However, the passive transmembrane transport of gold particles studied with liposomes mimicking biological membrane (Banerji and Hayes, 2007) had revealed that gold particles did not diffuse through the lipid membrane suggesting that interactions with lipid membrane are likely required.

Adhesion of colloidal particles onto giant vesicles based on electrostatic interactions induced the coverage of the particle by lipid membrane. This coverage was not limited to the vesicle-bead contact but rather extended to the entire bead while remaining attached to the vesicle periphery (Fery et al., 2003). Theoretical models have been proposed to predict adhesion and wrapping mechanism for colloid–vesicle complexes. The penetration is possible for large vesicle radii compared to the particle radii whereas for small vesicles (R = 300 nm) it will not be complete for any colloid radius (Deserno and Gelbart, 2002). Simulations of adhesive interaction of lipid bilayers with a spherical particle have shown the inducement of an engulfing process (Smith et al., 2007; Reynwar et al., 2007). The particle is wrapped by the membrane, but may remain tethered to it. To have a complete engulfing process, the presence of phase-separated membrane domains is needed to promote fission, allowing the particle detachment from the larger membrane (Smith et al., 2007). Other simulations based on modeling thermodynamics of interactions between charged nanoparticles and lipid membrane, confirmed the deposition of a lipid bilayer around the particle triggering the formation of a hole

Abbreviations: TEM, transmission electron microscopy; ET, electron tomography; DOPC, 1,2-dioleoyl-*sn*-glycero-3-phosphocholine; SLB, supported lipid bilayer; LUV, large unilamellar vesicle; SNP, silica nanoparticle; AFM, atomic force microscopy.

* Corresponding author. Fax: +33 5 40002200.
E-mail address: o.lambert@cbmn.u-bordeaux.fr (O. Lambert).
[1] Present address: European Molecular Biology Laboratory, Meyerhofstrasse 1, D–69117 Heidelberg, Germany.

1047-8477/$ - see front matter © 2009 Elsevier Inc. All rights reserved.
doi:10.1016/j.jsb.2009.07.006

in the membrane (Ginzburg and Balijepalli, 2007) as observed by atomic force microscopy (AFM) on supported lipid bilayer (SLB) interacting with dendrimer particles. In spite of these multidisciplinary approaches, nanoparticle internalization is not fully understood and the mechanism by which the particle can transmigrate across cell membrane or model membrane remains a matter of debate.

Recently, interactions between lipid membrane and solid support have been investigated through the deposition of small lipid vesicles on large solid support i.e. cm^2-size monolithic substrates (glass, silica, mica or titanium dioxide), μm-size and nm-size silica beads (Richter et al., 2003; Reimhult et al., 2003; Rossetti et al., 2005; Cremer and Boxer, 1999; Linseisen et al., 1997; Baksh et al., 2004; Mornet et al., 2005). The strong adhesion of lipid vesicles on solid surfaces induces vesicle rupture and leads to the formation of a continuous, free-defect SLBs. The interaction of small unilamellar liposomes on silica nanoparticles (SNP) detailed by cryo-transmission electron microscopy (cryo-TEM) revealed the vesicle spreading and the formation of the so called nanoSLB faithfully following the surface of the particles (Mornet et al., 2005).

In the present study, we focus on the interaction of SNPs with large unilamellar liposomes (LUV) using cryo-TEM and cryo-electron tomography (cryo-ET) – a well-suited method for determining 3D assemblies of SNPs (Taveau et al., 2008). We evidence a complete internalization of SNP into LUV mediated by lipid membrane spreading around SNP surface. A transmigration mechanism involving adhesion and bending energies is proposed based on visualization of intermediate steps.

2. Materials and methods

2.1. Materials

All chemical products were purchased from Sigma. Absolute ethanol (J.T. Baker) and ammonia (Carlo Erba) were used as received. Water was deionized (resistivity higher than 18 MΩ). DOPC Lipid was purchased from Avanti polar lipids.

2.2. Synthesis and surface modification of gold and silica-based nanoparticles

Gold nanoparticles were prepared by citrate reduction method derived from the protocol of Turkevich et al. (1951) and optimised in order to obtain 10 nm diameter nanoparticles with a highly monodisperse size distribution (Mornet and Brisson, 2007; Renault et al., 2008). The gold surface functionalization based on the exchange of citrate ligand by a hetero-bifunctional PEO macromolecule bearing a thiol (–SH) group in ω position and amine (–NH2) group in α position was carried out following the method previously described (Mornet and Brisson, 2007; Renault et al., 2008). The final concentration of aminated gold nanoparticles was 4.8×10^{17} particles/l in ultrapure water.

The synthesis of silica-based nanoparticles (SNP) were prepared from a method derived from the Stöber process (Stöber et al., 1968) and previously described for 110 nm diameter SNPs (Mornet et al., 2005). Others sizes of SNPs containing 7 nm diameter maghemite nanocrystals in core–shell morphology have been also produced in the aim of this study by seed growth process. Maghemite nanoparticles prepared by coprecipitation method (Massart, 1981) were used as seeds in the reaction media for the growing of the silica shell in order to generate a large set of SNPs with controlled sizes according to the method previously reported (Mornet et al., 2007). For the study of the size effect on the internalization process, 15, 30, 40, 65 and 190 nm diameter $\gamma Fe_2O_3@SiO_2$ nanoparticles were generated. All SNPs were diluted to a concentration of 1 g/L in 10 mM Hepes buffer at pH 7.4.

2.3. Liposome preparation

LUVs were prepared by the reverse phase evaporation technique in 150 mM NaCl 10 mM Hepes pH 7.4, followed by filtration of the preparation (10 mg/ml) through a polycarbonate membrane, successively at 1, 0.4 and 0.2 μm (Lambert et al., 1998).

2.4. Sample preparation

For SNP internalization experiments, SNPs (100 μg/ml) were mixed for 1 h at room temperature with LUV (45 μg/ml). In these conditions, the lipid bilayer surface is expected to be in 10 times in excess compared to SNP surface (Mornet et al., 2005). For the inhibition experiments involving the aminated gold beads, liposomes and gold beads were first mixed together. An equal volume of SNP solution was then added to maintain the same final concentration as above.

2.5. Cryo-electron microscopy and 3D tomography

A 5 μl sample was deposited onto a holey carbon coated copper grid; the excess was blotted with a filter paper, and the grid was plunged into a liquid ethane bath cooled with liquid nitrogen (Leica EM CPC). Specimens were maintained at a temperature of approximately −170 °C, using a cryo holder (Gatan), and were observed with a FEI Tecnai F20 electron microscope operating at 200 kV and at a nominal magnification of 50,000× under low-dose conditions. Images were recorded with a 2 k × 2 k slow scan CCD camera (Gatan).

For cryo-electron tomography, tilt-series were collected automatically on both FEI Tecnai F20 and Tecnai G2 Polara from −60° to +60° with 2° angular increment using the FEI tomography software. Images were recorded on CCD camera at a defocus level between −8 and −4 μm. The pixel size at the specimen level varied between 0.5 and 0.36 nm. For image processing, using colloidal gold particles as fiducial markers, the 2D projection images, binned by a factor of two, were aligned with the IMOD software (Mastronarde, 1997), and then tomographic reconstructions were calculated by weighted back-projection using Priism/IVE package (Chen et al., 1996).

2.6. Segmentation and radius measurements

As delineation of contours and surfaces is a tedious and error-prone for humans, a semi-automated procedure was developed using the continuous maximum flow automated segmentation technique of Appleton and Talbot (2006). It requires a source, a sink and computes a metric-weighted, continuous domain, globally optimal minimal cut between them. This method interpolates missing edges optimally, including topological and shape constraints. The 3D source seeds were obtained incrementally from 2D axial sections with strong edges via manual gradient thresholding and linked together for topology preservation. The sink was provided by the feature's bounding box. The scalar metric was computed from the image gradient as $1/(1 + |\nabla I|^2)$, following Caselles et al. (1997). Segmentation software was produced by the authors. The resulting segmentation figures were produced with Amira.

Curvature was computed from the resulting segmentation by finding its Euclidean medial axis extremities (Couprie et al., 2007) in the region of interest, and fitting the osculating sphere to the external membrane surface at each extremity. The reported

curvature radius is the median value of all measurements in the region of interest, and is sub-voxel accurate.

3. Results and discussion

In a first part, we describe experiments carried out in a controlled environment allowing us to reproduce the nanoparticle transmigration as observed in red blood cells and in giant vesicles. By adjusting LUV and SNP sizes, the engulfing process was limited to one SNP event or even prevented. In a second part for slowing down the process and visualizing intermediate steps, aminated gold beads were added providing a better understanding of the mechanism underlying the SNP transmigration.

3.1. SNP internalization into liposome

This study aimed at analyzing by cryo-TEM and cryo-ET interactions of SNP with LUV mimicking cell membrane. After mixing 40 nm SNPs mixed with LUV, liposomes appeared loaded with several SNPs (Fig. 1A). To ensure that SNPs were unambiguously internalized into the liposome and not bound to the membrane surface, 3D architectures of SNP-containing liposomes were determined by cryo-ET. SNPs were definitively internalized into the liposomes regarding the extracted central slice and the volume surface representation (Fig. 1B, C). Clearly, SNPs were embedded in ice layer whose thickness was estimated to 200 nm regarding to the distance between ice contaminants present at both surfaces of the ice layer (black arrows). The liposome was trapped within the ice layer and must have kept its overall closed structure although the upper and lower parts of liposome were not visible due to the missing wedge artefact. The three SNPs, located in equatorial plane (coloured in yellow in Fig. 1C) were far enough from the LUV boundaries to be considered as complete internalized SNPs without any interaction with the LUV membrane. To detail the mechanism of SNP entry, it deserves further experiments involving single internalization event of SNP for the sake of clarity.

For this purpose, 110 nm SNPs were mixed with LUVs. A large number of liposomes exhibited one or two SNPs in the centre (Fig. 2A). At high magnification, SNPs were surrounded by the lipid membrane of the liposome forming a closed circle (Fig. 2B, C). More importantly they were wrapped by an electron-dense ring that corresponds to a nanoSLB (white arrows in Fig. 2B, C) according to our previous work on formation of SLB on silica nanoparticles (Mornet et al., 2005). These results suggest that SNPs are internalized into liposome according to an invagination process as schematically represented in Fig. 2E and not by a passive diffusion across the membrane. About 20% of nanoparticles were involved in the internalization process. The other nanoparticles were solely covered by a SLB corresponding to nanoSLBs (asterisk Fig. 2B) (Mornet et al., 2005).

In addition, liposomes composed of two concentric lipid bilayers were able to entrap SNP sandwiched between their two lipid membranes (Fig. 2D). This original engulfing process revealed that only the outer membrane triggered the SNP internalization and that this process did not involve both membranes. The inner membrane is deformed by the particle entry. These events give also evidence that a SNP already covered by a SLB cannot enter into a liposome.

3.2. Topology of liposome-internalized SNP by cryo-ET

Among all SNPs engaged in the engulfing process, few of them were observed not completely internalized. The 3D structure determination of such assemblies allows us to provide a 3D

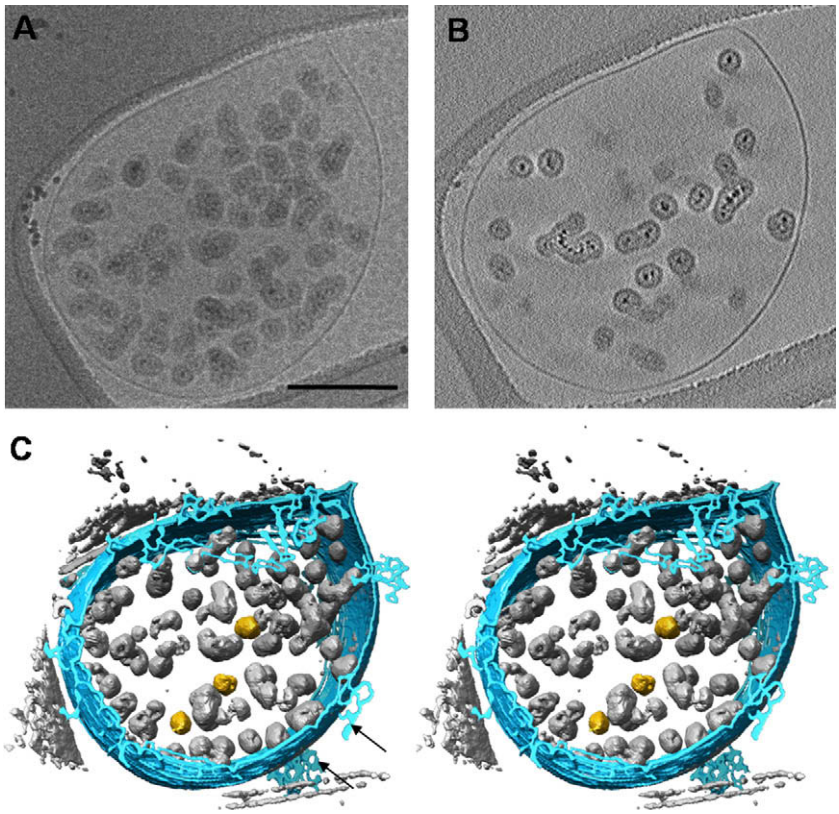

Fig. 1. Cryo-ET of 40 nm SNP internalization into LUVs. (A) Cryo-EM image at 0° tilt. (B) Extracted section of the calculated tomogram. (C) Parallel-eye stereoscopic view of the segmented tomogram. Lipid membrane and SNPs are coloured respectively in blue and light gray. Three yellow SNPs are highlighted due to their equatorial localization. Ice contaminants (black arrows) present on both sides of ice layer provide an estimation of its thickness. Scale bar 200 nm.

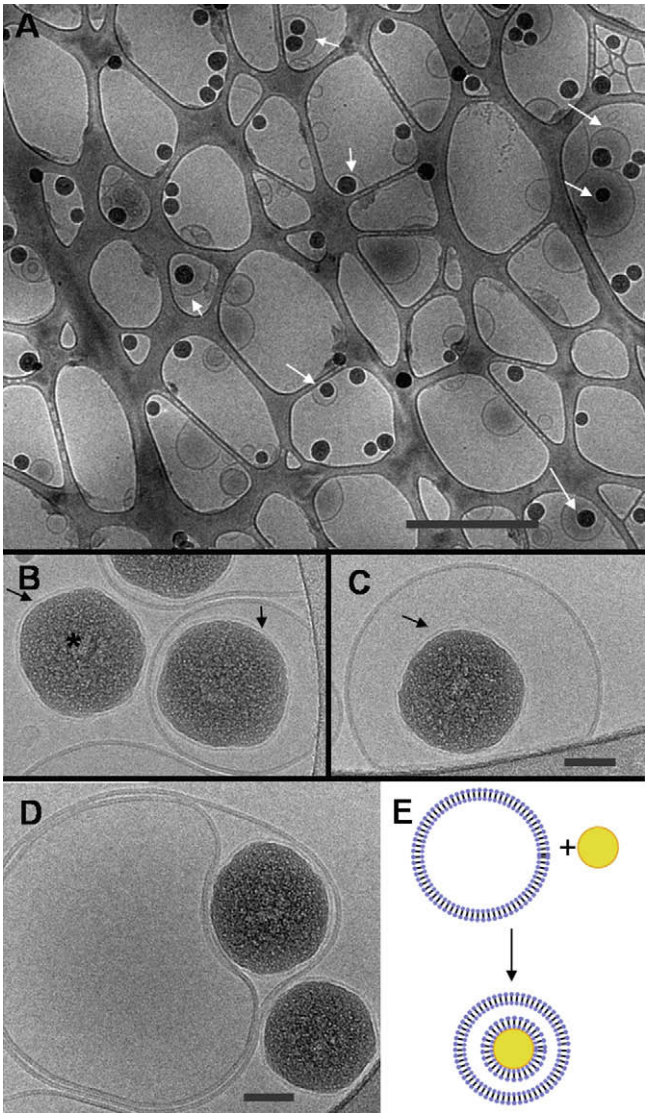

Fig. 2. Internalization of SNPs into LUVs. (A) Cryo-EM field showing SNPs entrapped within DOPC vesicles (white arrows). (B, C) Typical high magnification images of liposomes containing engulfed SNPs appearing as dense grainy spheres that are covered by a SLB (black arrows). SNPs covered only with a nanoSLB are also visible (asterisk). (D) In the presence of a liposome made of two lipid membranes, SNP is wrapped by only the outer lipid membrane triggering SNP internalization. The inner liposome is not involved in this process. (E) Scheme of SNP internalized into LUV. During this process SNP is wrapped by a SLB. Scale bars 1 μm (A) and 50 nm (B–D) respectively.

detailed organization of the vesicle spreading around SNP (Fig. 3A–C). The vesicle almost fully covered SNP. SLB was clearly visible on the extracted slices (white arrows in Fig. 3B, C). The membrane boundaries of the vesicle demarcated on the silica surface an oval-shaped area (black arrow in Fig. 3A). The shortest distance between membrane edges was about 9 nm (Fig. 3B). To pursue the internalization process, the most likely step would be the extension of the vesicle spreading to reduce the size of the oval-shaped area up to form a structure similar to a membrane neck described previously (Kozlovsky and Kozlov, 2003; Markvoort et al., 2007) leading to vesicle fission and a complete internalization (step 3 in Fig. 3G). The edges had a round-shaped structure inducing a strong curvature of the lipid bilayer. This membrane deformation was estimated by the measurement of the radius a of a circle delineated by the membrane curvature. A mean value of $a = 6 \pm 1$ nm was calculated from several slices using an automatic procedure (see Section 2).

At first sight, the observation of highly curved necks seems rather surprising and deserves a few comments. In a continuum description, the elastic energy associated with a given conformation of a tensionless bilayer is shown in Eq. (1) (Leibler, 2004)

$$E = \frac{1}{2}k_b \int dS\left(\frac{1}{R_1}+\frac{1}{R_2}\right)^2 + k_g \int dS \frac{1}{R_1 R_2} \quad (1)$$

with R_1 and R_2 the local curvature radii. The integrals extend over the whole surface of the liposome. The elastic constants k_b and k_g are the bending and Gaussian rigidity, respectively. Both have the dimension of an energy. For DOPC bilayers, the bending rigidity is typically $k_b \sim 8 \times 10^{-20}$ J at room temperature (Pan et al., 2008). The Gaussian rigidity is more difficult to measure since it is related to the topology of the membrane: in fact, integrating the second contribution over any closed surface yields to a constant value $4\pi k_g$ (Leibler, 2004) so that this contribution is not related to the local shape of the liposome. According to the above expression, one would naively expect the highly curved region seen on Fig. 3A–C to give rise to a large bending energy. Indeed, since the a radius of the membrane edge is of the order of the neck size, both curvature radii should lead to equally important contributions. However, the point is that the two curvatures actually contribute with an *opposite sign* to the mean curvature. The bending energy of the neck is therefore vanishingly small, scaling linearly with the membrane edge radius (Fourcade et al., 1994).

3.3. Influence of the size of nanoparticle

As previously mentioned, the SNP size influenced the engulfing process (Figs. 1 and 2). For a more complete study, SNPs with various diameters (from 15 to 190 nm) were mixed DOPC liposomes (Fig. 4). The transmigration process was observed with 190 nm SNPs engulfed into large vesicles (Fig. 4A). For larger SNPs, cryo-TEM observation was less suitable due to ice thickness leading to a lack of contrast. To study the engulfing process for small SNPs, we used maghemite silica core–shell particles providing a contrast higher than pure silica particles, which was very convenient for very small particles. SNPs with diameter of 65 and 30 nm were entrapped into liposomes as well, as evidenced with the SLB surrounding the particles (Fig. 4B–D). However, SNPs with a diameter of about 15–20 nm remained bound to the outer surface of the liposome. Moreover, they did not exhibit at their periphery typical densities corresponding to SLB. Although SNPs interacted with DOPC lipid membranes in the same way as the larger ones, the adhesive strength was not sufficient to induce a curvature of the lipid membrane and then to trigger the engulfing process (Fig. 4E, F). Then SNPs with diameter larger than 30 nm were engulfed inside the liposome whereas those with diameter 15–20 nm were not. This size effect was in agreement with recent AFM study revealing a threshold for the membrane spreading over nanoparticles (Roiter et al., 2008). This size dependence is a consequence of the balance between adhesive and elastic forces. The adhesive energy per unit area w that controls encapsulation is a subtle combination of several short-range interactions: screened electrostatics, van der Waals, hydration and steric forces, ... (Israelachvili, 1992). Complete coverage of the particle then occurs when the total adhesion energy overcomes the energy cost associated with the bending of the bilayer. For tensionless membranes, this criterion leads to a critical particle radius $R_c = (2k_b/w)^{1/2}$ (Deserno and Bickel, 2003; Lipowsky and Döbereiner, 1998). Colloids with radius smaller than R_c are expected to remain bound outside of the liposome, whereas full wrapping occurs above R_c. The knowledge of intramolecular forces would in principle give us the value

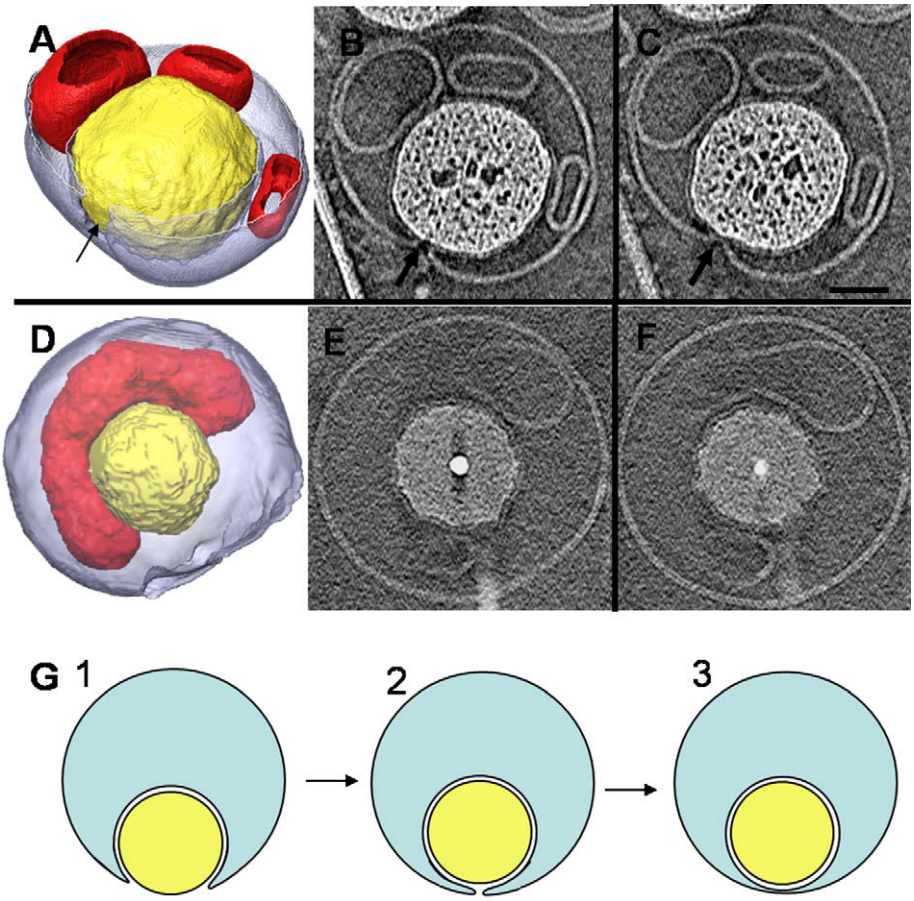

Fig. 3. Mechanism of an engulfed SNP into a liposome. (A–C) Cryo-ET of SNP engaged in the internalization process. Isosurfaces of segmented tomogram showing the overall architecture of the partially engulfed particle (yellow) into the large liposome (blue) and small liposomes present within the liposome in red (A). The SLB is clearly visible around the silica particle. Note the open area formed by the vesicle boundaries (black arrows) depicted on two tomographic 0.73 nm-thick slices (B,C). (D–F) Isosurfaces of a double liposome showing the fully internalized SNP (yellow), the inner liposome in red (D). SLB is visible around SNP on two 2.5 nm extracted slices distant from 10 nm (E, F). (G) Scheme describing the internalization in three steps: step 1: the vesicle spreading, step 2: Almost complete engulfing and step 3: Fully internalized particle. Scale bar 50 nm.

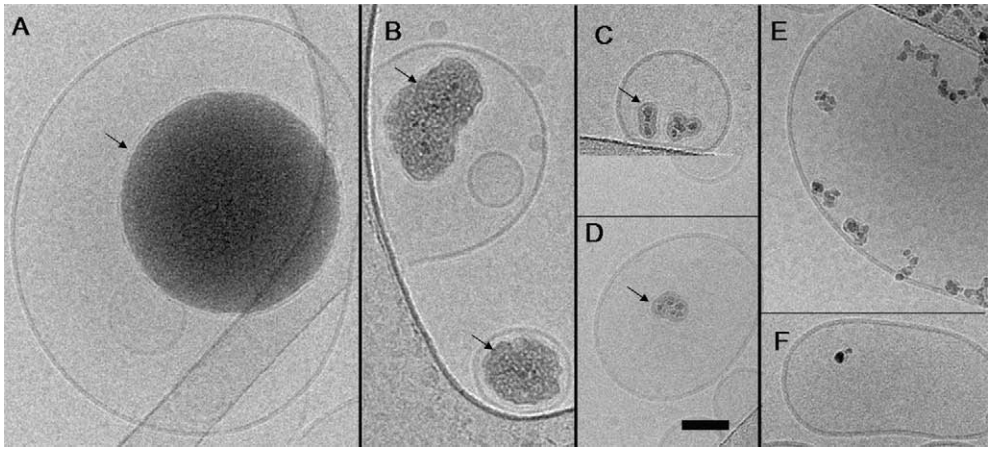

Fig. 4. Influence of SNP diameter on the engulfing process. The engulfing process has been studied for various SNP sizes. SNPs with a diameter of 190 nm (A), 65 nm (B) and 30 nm (C, D) respectively are internalized as evidenced by the presence of SLB surrounding SNP surface (black arrows). (E, F) 15 nm SNPs remain attached to the outer surface of the liposomes. Scale bar 50 nm.

of w and therefore of the critical radius. However, the various contributions to the adhesion energy are not easily evaluated. We can still estimate w from the experimental data (Fig. 4) leading to a R_c in the range of 10–15 nm, corresponding to an adhesive strength w of a few mJ/m^2 (or erg/cm^2) – a value comparable to usual interfacial energies (Israelachvili, 1992).

3.4. Visualization of intermediate steps of SNP internalization using gold beads

In order to get insight into the mechanism of internalization, attempts to observe intermediate steps by freezing samples at different incubation times after mixing SNPs and liposomes were not successful mainly because the process occurred in a time laps faster than that can be experimentally analyzed. To overcome this drawback, we developed a method that blocks or slows down the engulfing process with the use of 10 nm positively charged gold nanoparticles. Gold nanoparticles were mixed with SNPs at a gold bead to SNP ratio r equal to 200 fully covering SNP surfaces. Then, their interactions with SNPs prevented liposome spreading onto silica surface (Fig. 5A). Therefore, the coverage of SNP with liposomes in the presence of gold beads was studied by cryo-TEM. The gallery revealed intermediate steps of SNP covered by the liposome engaged in the engulfing process (Fig. 5B–F). LUVs were observed partially spread onto SNP, as schematically drawn in Fig. 3G. The interactions of gold beads with SNP were strong enough to block the vesicle spreading. This process was stopped at different stages which were directly related to the amount of gold beads attached to SNP. These results definitively prove that SNP is entrapped into the liposome via an internalization process driven by the spreading forces of the lipid bilayer on the silica surface (step 1, Fig. 3G). Intermediate steps were also observed with liposomes made of two concentric lipid layers and revealed that the outer lipid membrane creeps up the silica surface inducing the deformation of the inner membrane (white arrows in Fig. 5E, F). Then, the outer membrane initiates the engulfment of SNP driven by strong adhesive interactions. To fully internalize SNP, the ultimate stage corresponds to the fission of the edges of the vesicle membrane creeping on the SNP surface (steps 2–3 in Fig. 3G) (Deserno and Gelbart, 2002).

Besides adhesion and bending energies, the notion of Gaussian rigidity has to be invoked in order to explain the complete internalization of SNP. Indeed, the fission process involves a modification of the topology (separation of the vesicle/colloid complex from the large liposome, step 3 in Fig. 3G). Although there is no available estimation of k_g for DOPC bilayers, the spontaneous fission of the liposome certainly reflects a negative value of the Gaussian rigidity. This assertion is fully consistent with the criterion for a stable vesicle phase: $k_g < -2k_b$ (Leibler, 2004).

In summary, our results indicate that the full internalization of SNP into LUVs is mediated by an invagination process as shown by the tomograms of intermediate steps. Our success at observing this process at nanometer scale provides new insights into the transmigration mechanism regarding information retrieved from giant vesicles (Fery et al., 2003; Fleck and Netz, 2004; Benoit and Saxena, 2007; Livadaru and Kovalenko, 2006; Dietrich et al., 1997; Koltover et al., 1999). In particular, we have shown that SNPs (30–190 nm in diameter) are fully internalized into vesicles whose diameters range from 100 to 300 nm, well below the 300 nm threshold estimated by Deserno and Gelbart (2002). We have also evidenced that complete internalization of nanoparticle does occur with pure DOPC lipids in the fluid phase, meaning that phase-separated membrane domains are not a prerequisite for membrane fission, as it was recently suggested (Smith et al., 2007). The idea that SNP may induce the rupture of the lipid membrane and the formation of nanosized hole (Ginzburg and Balijepalli, 2007) is not supported by our results either. Note however that different

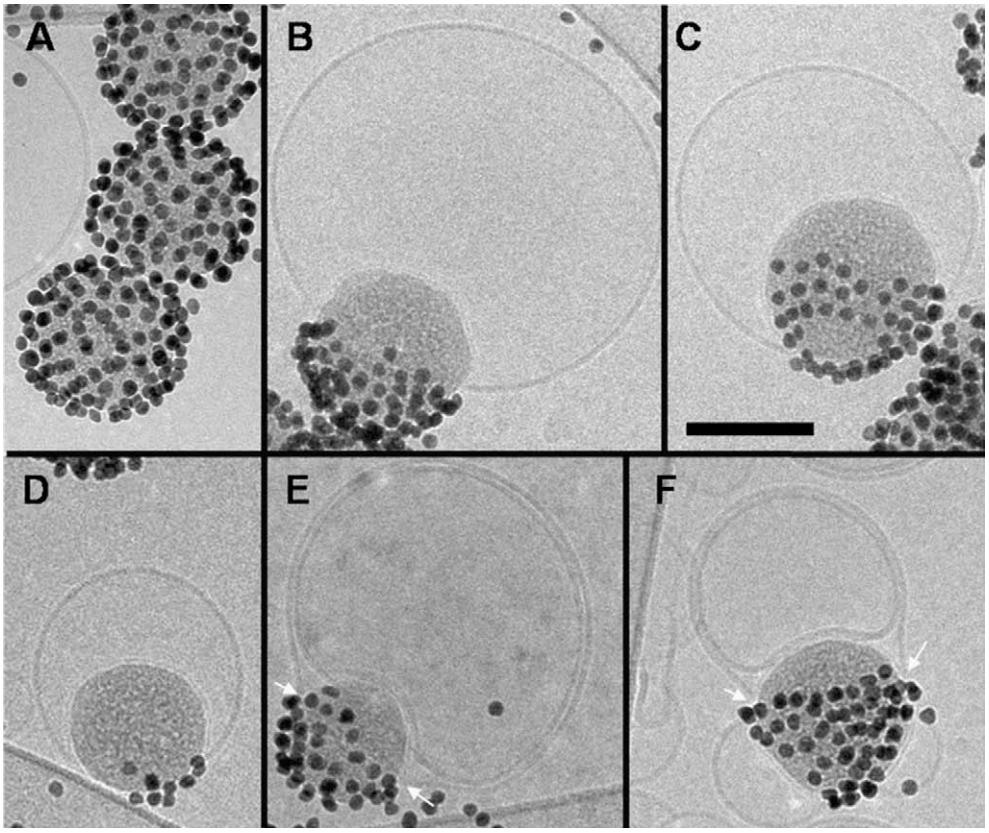

Fig. 5. Internalization process prevented by gold beads. (A) Gold beads fully covering SNP prevents SNP/liposome interaction. (B–D) Gallery of cryo-EM images revealing intermediates steps of vesicle spreading (step 1 in Fig. 3G). The use of positively charged gold beads allows blocking the DOPC liposomes spreading on silica surface. (E, F) Intermediate steps are observed on double membrane liposomes. The outer liposome creeps up the nanoparticle surface (white arrows) progressively internalizing SNP which pushes the inner liposome. Scale bar 50 nm.

translocation pathways may occur in experiments on SLBs, in which the underlying support is expected to have a valuable influence (Mecke et al., 2005; Leroueil et al., 2008). In the case of SLB, it is possible that the mica support (usually negatively charged) used for AFM imaging may have an attractive effect on the cationic nanoparticles beyond the SLB and then facilitates the subsequent hole formation.

4. Conclusion

In the present study, we demonstrate that nanoparticles interacting strongly with lipid membrane can be transported through it via an invagination process without the need of supplementary energy. It is now of importance to investigate their interactions with cell membrane at nanometer scale. This invagination process evidenced on model membrane could be helpful for a better understanding of the underlying mechanisms involved in nanoparticle cellular uptake, including passive or active transports and processes associated with their cytotoxicity.

Acknowledgments

O. Le Bihan is recipient of Ph D fellowships from Vaincre la Mucovicidose. S. Trépout was recipient of Ph D fellowships from French Ministry of Education and Research and Technology (MENRT). The authors thank J. Lai Kee Him for technical assistance. This work has been supported in part by ANRS (AO2007-2) and Conseil Régional d'Aquitaine (20071302007) Grants.

References

Appleton, B., Talbot, H., 2006. Globally minimal surfaces by continuous maximal flows. IEEE Trans. Pattern Anal. Mach. Intell. 28, 106–118.
Baksh, M.M., Jaros, M., Groves, J.T., 2004. Detection of molecular interactions at membrane surfaces through colloid phase transitions. Nature 427, 139–141.
Banerji, S.K., Hayes, M.A., 2007. Examination of nonendocytotic bulk transport of nanoparticles across phospholipid membranes. Langmuir 23, 3305–3313.
Benoit, J., Saxena, A., 2007. Spherical vesicles distorted by a grafted latex bead: an exact solution. Phys. Rev. E 76, 041912.
Caselles, V., Kimmel, R., Sapiro, G., 1997. Geodesic active contours. Int. J. Comput. Vis. 22, 61–79.
Chen, H., Hughes, D.D., Chan, T.A., Sedat, J.W., Agard, D.A., 1996. IVE (Image Visualization Environment): a software platform for all three-dimensional microscopy applications. J. Struct. Biol. 116, 56–60.
Couprie, M., Coeurjolly, D., Zrour, R., 2007. Discrete bisector function and Euclidean skeleton in 2D and 3D. Image Vis. Comput. 25, 1543–1556.
Cremer, P., Boxer, S.G., 1999. Formation and spreading of lipid bilayers on planar glass supports. J. Phys. Chem. B 103, 2554–2559.
Deserno, M., Bickel, T., 2003. Wrapping of a spherical colloid by a fluid membrane. EPL 62, 767–773.
Deserno, M., Gelbart, W.M., 2002. Adhesion and wrapping in colloid–vesicle complexes. J. Phys. Chem. B 106, 5543–5552.
Dietrich, C., Angelova, M., Pouligny, B., 1997. Adhesion of Latex spheres to giant phospholipid vesicles: statics and dynamics. J. Phys. II (France) 7, 1651–1682.
Fery, A., Moya, S., Puech, P.-H., Brochart-Wyart, F., Mohwald, H., 2003. Interaction of polyelectrolyte coated beads with phospholipid vesicles. C. R. Phys. 4, 259–264.
Fleck, C., Netz, R.R., 2004. Electrostatic colloid–membrane binding. EPL 67, 314–320.
Fourcade, B., Miao, L., Rao, M., Wortis, M., Zia, R.K.P., 1994. Scaling analysis of narrow necks in curvature models of fluid lipid-bilayer vesicles. Phys. Rev. E 49, 5276–5286.
Geiser, M., Rothen-Rutishauser, B., Kapp, N., Schürch, S., Kreyling, W., Schulz, H., Semmler, M., Im Hof, V., Heyder, J., Gehr, P., 2005. Ultrafine particles cross cellular membranes by nonphagocytic mechanisms in lungs and in cultured cells. Environ. Health Perspect. 113, 1555–1560.
Ginzburg, V.V., Balijepalli, S., 2007. Modeling the thermodynamics of the interaction of nanoparticles with cell membranes. Nano Lett. 7, 3716–3722.
Israelachvili, J.N., 1992. Intermolecular and Surface Forces. Academic Press, London.
Koltover, I., Rädler, J.O., Safinya, C.R., 1999. Membrane mediated attraction and ordered aggregation of colloidal particles bound to giant phospholipid vesicles. Phys. Rev. Lett. 82, 1991–1994.
Kozlovsky, Y., Kozlov, M.M., 2003. Membrane fission: model for intermediate structures. Biophys. J. 85, 85–96.
Lambert, O., Levy, D., Ranck, J.L., Leblanc, G., Rigaud, J.L., 1998. A new 'gel-like' phase in dodecyl maltoside–lipid mixtures: implications in solubilization and reconstitution studies. Biophys. J. 74, 918–930.
Leibler, S., 2004. In: Nelson, D., Piran, T., Weinberg, S. (Eds.), Statistical Mechanics of Membranes and Surfaces. Word Scientific, Singapore.
Leroueil, P.R., Berry, S.A., Duthie, K., Han, G., Rotello, V.M., McNerny, D.Q., Baker Jr., J.R., Orr, B.G., Holl, M.M., 2008. Wide varieties of cationic nanoparticles induce defects in supported lipid bilayers. Nano Lett. 8, 420–424.
Linseisen, F.M., Hetzer, M., Brumm, T., Bayerl, T.M., 1997. Differences in the physical properties of lipid monolayers and bilayers on a spherical solid support. Biophys. J. 72, 1659–1667.
Lipowsky, R., Döbereiner, H.-G., 1998. Vesicles in contact with nanoparticles and colloids. EPL 43, 219–225.
Livadaru, L., Kovalenko, A., 2006. Fundamental mechanism of translocation across liquidlike membranes: toward control over nanoparticle behavior. Nano Lett. 6, 78–83.
Markvoort, A.J., Smeijers, A.F., Pieterse, K., van Santen, R.A., Hilbers, P.A., 2007. Lipid-based mechanisms for vesicle fission. J. Phys. Chem. B 111, 5719–5725.
Massart, R., 1981. Preparation of aqueous magnetic liquids in alkaline and acidic media. IEEE Trans. Magn. 17, 1247–1248.
Mastronarde, D.N., 1997. Dual-axis tomography: an approach with alignment methods that preserve resolution. J. Struct. Biol. 120, 343–352.
Mecke, A., Majoros, I.J., Patri, A.K., Baker Jr., J.R., Holl, M.M., Orr, B.G., 2005. Lipid bilayer disruption by polycationic polymers: the roles of size and chemical functional group. Langmuir 21, 10348–10354.
Mornet, S., Lambert, O., Duguet, E., Brisson, A., 2005. The formation of supported lipid bilayers on silica nanoparticles revealed by cryoelectron microscopy. Nano Lett. 5, 281–285.
Mornet, S., Elissalde, C., Bidault, O., Weill, F., Sellier, E., Nguyen, O., Maglione, M., 2007. Ferroelectric-based nanocomposites: toward multifunctional materials. Chem. Mater. 19, 987–992.
Mornet, S., Brisson, A., 2007. Functionalization of gold nanoparticles with oriented proteins. Application to the high density labelling of cell membranes. Patent no. WO2007122259.
Nel, A., Xia, T., Mädler, L., Li, N., 2006. Toxic potential of materials at the nanolevel. Science 311, 622–627.
Pan, J., Tristam-Nagle, S., Kucerka, N., Nagle, J.F., 2008. Temperature dependence of structure, bending rigidity, and bilayer interactions of dioleoylphosphatidylcholine bilayers. Biophys. J. 94, 117–124.
Rothen-Rutishauser, B.M., Schürch, S., Haenni, B., Kapp, N., Gehr, P., 2006. Interaction of fine particles and nanoparticles with red blood cells visualized with advanced microscopic techniques. Environ. Sci. Technol. 40, 4353–4359.
Reimhult, E., Höök, F., Kasemo, B., 2003. Intact vesicle adsorption and supported biomembrane formation from vesicles in solution: influence of surface chemistry, vesicle size, temperature, and osmotic pressure. Langmuir 19, 1681–1691.
Renault, S., Baudrimont, M., Mesmer-Dudons, N., Gonzalez, P., Mornet, S., Brisson, A., 2008. Impacts of gold nanoparticle exposure on two freshwater species: a phytoplanktonic alga (*Scenedesmus subspicatus*) and a benthic bivalve (*Corbicula fluminea*). Gold Bull. 41, 116–126.
Reynwar, B.J., Illya, G., Harmandaris, V.A., Müller, M.M., Kremer, K., Deserno, M., 2007. Aggregation and vesiculation of membrane proteins by curvature-mediated interactions. Nature 447, 461–464.
Richter, R., Mukhopadhay, A., Brisson, A., 2003. Pathways of lipid vesicle deposition on solid surfaces: a combined QCM-D and AFM study. Biophys. J. 85, 3035–3047.
Roiter, Y., Ornatska, M., Rammohan, A.R., Balakrishnan, J., Heine, D.R., Minko, S., 2008. Interaction of nanoparticles with lipid membrane. Nano Lett. 8, 941–944.
Rossetti, F.F., Bally, M., Michel, R., Textor, M., Reviakine, I., 2005. Interactions between titanium dioxide and phosphatidyl serine-containing liposomes: formation and patterning of supported phospholipid bilayers on the surface of a medically relevant material. Langmuir 21, 6443–6450.
Smith, K.A., Jasnow, D., Balazs, A.C., 2007. Designing synthetic vesicles that engulf nanoscopic particles. J. Chem. Phys. 127, 084703.
Stöber, W., Fink, A., Bohn, E., 1968. Controlled growth of monodisperse silica spheres in the micron size range. J. Colloid Interface Sci. 26, 62–69.
Taveau, J.-C., Nguyen, D., Perro, A., Ravaine, S., Duguet, E., Lambert, O., 2008. New insights into the nucleation and growth of PS nodules on silica nanoparticles by 3D cryo-electron tomography. Soft Matter 4, 311–315.
Turkevich, J., Stevenson, P.C., Hillier, J., 1951. A study of the nucleation and growth processes in the synthesis of colloidal gold. Discuss. Faraday Soc. 11, 55–75.